

ESVM : An Open-source Electrostatic Vlasov-Maxwell Code

Michaël J TOUATI^{1, 2, 3}

¹ Department of Electrical Engineering, University of California Los Angeles, Los Angeles, CA 90095, USA ² Group of Lasers and Plasmas, IPFN, IST, Universidade de Lisboa, Lisbon, Portugal ³ Centro de Láseres Pulsados de Salamanca (CLPU), Edificio M5, Parque Científico, C/ Adaja 8, 37185 Villamayor, Salamanca, Spain (current affiliation)

DOI: [10.21105/joss.0XXXX](https://doi.org/10.21105/joss.0XXXX)

Software

- [Review](#) ↗
- [Repository](#) ↗
- [Archive](#) ↗

Editor: [Editor Name](#) ↗

Submitted: 01 January XXXX

Published: 01 January XXXX

License

Authors of papers retain copyright and release the work under a Creative Commons Attribution 4.0 International License ([CC BY 4.0](#)).

Summary

ESVM (ElectroStatic Vlasov-Maxwell) is a single species 1D-1V Vlasov-Maxwell Fortran 90 code parallelized with OpenMP that allows for the study of collisionless plasmas. Many finite volume numerical advection schemes (Godunov, 1959) are implemented in the code in order to discretize the Vlasov equation, namely : - the donor-cell scheme i.e. the downwind / upwind scheme (R. Courant et al., 1952) depending on the advection direction in each phase-space cell, - the Lax-Wendroff scheme (Lax & Wendroff, 1960), - the Fromm scheme (Fromm, 1968), - the Beam-Warming scheme (Beam & Warming, 1976), - the Van Leer scheme (Van Leer, 1977), - the minmod scheme (Roe, 1986), - the superbee scheme (Roe, 1986) and - two Monotonic Upwind-centered Scheme for Conservation Laws (MUSCL) (van Leer, 1979) schemes MUSCL2 (Crouseilles & Filbet, 2004) and MUSCL1 (Duclos et al., 2009).

Contrary to the linear second order Lax-Wendroff, Fromm and Beam-Warming schemes, the non-linear second order minmod, superbee, Van Leer and MUSCL schemes make use of a Total Variation Diminishing (TVD) non-linear flux limiter with the price of becoming a first order scheme in some phase-space cells to limit the numerical oscillations. The donor-cell scheme is a first order method and has the pros of limiting such eventual oscillations but the cons of being numerically less consistent and more diffusive too. In ESVM, the discretized Vlasov equation is coupled with the self-consistent Maxwell-Gauss equation or equivalently with the Maxwell-Ampere equation with Maxwell-Gauss equation computed at the first time step, only. While the second order Maxwell-Gauss solver needs a computationally expensive inversion of a tridiagonal matrix for the computation of the Poisson equation, the Maxwell-Ampere equation solver makes use of the faster second order finite difference Yee scheme (Yee, 1966). Both absorbing and periodic boundary conditions for both the particles and the fields are implemented. Python scripts, using the Matplotlib and Numpy packages, are provided to automatically extract and plot the stored simulation results. Compilation rules can be easily modified depending on the user compiler preferences using the provided makefile. It is however recommended to compile the code using the double-precision compiler option. Well known Plasma Physics academic cases, tools for testing the compilation and tools for checking the simulation parameters that are specified by the user in the input-deck are provided.

Statement of need

ESVM has been developed in order to adapt simulations to specific Plasma Physics problems by choosing the more adequate finite volume numerical advection scheme in order to compute the Vlasov equation phase-space advection derivatives and to choose between computing the

Maxwell-Gauss equation or the Maxwell-Ampere equation with Maxwell-Gauss equation computed at the first time step, only. The code aims at being used by the open-source Highly Parallel Computing (HPC) Plasma Physics community ranging from under or post-graduate students to teachers and researchers who usually use Particle-In-Cell (PIC) codes (Dawson, 1962) to study collisionless plasmas. Indeed, the PIC method may prohibit the study of Plasma Physical processes on large time scales and/or for very dense collisionless plasmas due to the statistical and numerical fluctuations of the computed quantities imposed by the use of a finite number of macroparticles. Also, plasma instabilities naturally develop in PIC codes, seeded by the available fluctuations spatial spectrum k -vector for which the instability growth rate is maximum and some small amplitude Plasma Physical processes may be hidden under the fluctuations level. Compared to the many open source PIC code such as (Derouillat et al., 2018) and semi-Lagrangian codes such as (de Buyl, 2014), there is no open source finite volume Vlasov codes in the literature that are not based on an expansion method such as (Tzoufras et al., 2011) (Touati et al., 2014) or (Joglekar & Levy, 2020). In addition, since the Vlasov equation is a conservation equation of the number of particle in the phase-space, using a finite volume method in order to compute the Vlasov equation presents the advantage of allowing for the use of numerical schemes that are numerically flux conserving and/or that ensure the distribution function positivity compared to other numerical methods. ESVM has already been used during courses for under and post-graduate students about the “numerical tools for laser-plasma interaction Physics” and it is currently used for theoretical Plasma Physics investigations.

Equations computed by ESVM

Plasma ions are assumed to be immobile with a homogeneous density n_i and fully ionized with an electrical charge Ze where Z is the plasma ion atomic number and e the elementary charge. The plasma electron distribution function $f_e(x, v_x, t)$ is computed by ESVM according to the plasma electron Vlasov equation

$$\frac{\partial f_e}{\partial t}(x, v_x, t) + \frac{\partial}{\partial x}(v_x f_e(x, v_x, t)) - \frac{\partial}{\partial v_x} \left(\frac{e}{m_e} E_x(x, t) f_e(x, v_x, t) \right) = 0 \quad (1)$$

that is self-consistently coupled with the Maxwell-Gauss equation

$$\frac{\partial E_x}{\partial x}(x, t) = 4\pi e (Zn_i - n_e(x, t)) \quad (2)$$

for the electrostatic field $E_x(x, t)$ or, equivalently, self-consistently coupled with the Maxwell-Ampere equation

$$\frac{\partial E_x}{\partial t}(x, t) = -4\pi j_e(x, t) \quad (3)$$

with Maxwell-Gauss equation Equation 2 computed at the simulation start $t = 0$, only. Indeed, by integrating the plasma electron Vlasov equation Equation 1 over the whole plasma electron velocity space $v_x \in [v_{x,\min}, v_{x,\max}]$, one gets the hydrodynamic equation of plasma electron number conservation

$$\frac{\partial n_e}{\partial t}(x, t) + \frac{\partial}{\partial x}(n_e v_e(x, t)) = 0, \quad (4)$$

which, when injected in the time derivative of Maxwell-Gauss equation Equation 2, provides the Maxwell-Ampere equation Equation 3 if Maxwell-Gauss equation Equation 2 is verified at the simulation start $t=0$. Here,

$$n_e(x, t) = \int_{v_{x,\min}}^{v_{x,\max}} f_e(x, v_x, t) dv_x, \quad (5)$$

$$v_e(x, t) = \frac{1}{n_e(x, t)} \int_{v_{x,\min}}^{v_{x,\max}} f_e(x, v_x, t) v_x dv_x \quad (6)$$

78 and

$$j_e(x, t) = -en_e(x, t)v_e(x, t) \quad (7)$$

79 are the plasma electron density, mean velocity and electrical charge current, respectively.
80 ESVM also computes the plasma electron thermal velocity $v_{T_e}(x, t)$ defined according to the
81 plasma electron internal energy density

$$u_{T_e}(x, t) = \frac{n_e(x, t)}{2} m_e v_{T_e}(x, t)^2 = \frac{m_e}{2} \int_{v_{x, \min}}^{v_{x, \max}} f_e(x, v_x, t) (v_x - v_e(x, t))^2 dv_x. \quad (8)$$

82 For example, in 1D plasmas at local Maxwell-Boltzmann equilibrium, $v_{T_e}(x, t) =$
83 $\sqrt{k_B T_e(x, t)/m_e}$ where k_B is the Boltzmann constant, $T_e(x, t)$ is the local electron
84 temperature and m_e the electron mass. Maxwell-Gauss equation Equation 2 is computed by
85 using the electrostatic potential definition

$$\frac{\partial \Phi}{\partial x}(x, t) = -E_x(x, t) \quad (9)$$

86 that gives the Poisson equation

$$\frac{\partial^2 \Phi}{\partial x^2}(x, t) = -4\pi e (Zn_i - n_e(x, t)) \quad (10)$$

87 for the electrostatic potential Φ when injected in the Maxwell-Gauss equation Equation 2.
88 When the simulation is running, ESVM stores at every time steps and displays on the terminal
89 at every dumped time steps t_d the total plasma electron internal and kinetic energy (assuming
90 simulations with an area unit perpendicular to the x -axis of λ_{Debye}^2) and the total electrostatic
91 energy in the simulation box $x \in [x_{\min}, x_{\max}]$

$$U_{T_e}(t_d) = \lambda_{\text{Debye}}^2 \int_{x_{\min}}^{x_{\max}} u_{T_e}(x, t_d) dx, \quad (11)$$

92

$$U_{K_e}(t_d) = \lambda_{\text{Debye}}^2 \int_{x_{\min}}^{x_{\max}} n_e(x, t) \frac{m_e v_e(x, t_d)^2}{2} dx \quad (12)$$

93 and

$$U_{E_x}(t_d) = \lambda_{\text{Debye}}^2 \int_{x_{\min}}^{x_{\max}} \frac{E_x(x, t_d)^2}{8\pi} dx, \quad (13)$$

94 respectively as well as the total energy area density

$$U_{\text{tot}}(t_d) = U_{T_e}(t_d) + U_{K_e}(t_d) + U_{E_x}(t_d) \quad (14)$$

95 in order to check the energy conservation in the simulation.

96 ESVM units

97 The code units consist in the commonly used electrostatic units : the electron mass m_e for
98 masses, the elementary charge e for electrical charges, the inverse of the Langmuir plasma
99 electron angular frequency $\omega_p = \sqrt{4\pi Zn_i e^2/m_e}$ for times, the Debye electron screening length
100 $\lambda_{\text{Debye}} = v_{T_{e0}}/\omega_p$ and the constant electron density $n_0 = Zn_i$ for spatial densities. $v_{T_{e0}}$ is
101 therefore an important unit parameter of normalization since it fixes indirectly the space unit.
102 It can be defined more generally as the initial plasma electron velocity distribution standard
103 deviation if the plasma is not initialized at Maxwell-Boltzmann thermodynamic equilibrium;
104 cf. Equation 8. Injecting these units in the equations computed by the code, one deduces the
105 resulting normalized electrostatic field and electron distribution function that consequently
106 reads $\underline{E_x} = eE_x/m_e\omega_p v_{T_{e0}}$ and $\underline{f_e} = f_e v_{T_{e0}}/n_0$, respectively.

ESVM numerical stability

The spatial grid cells should be chosen lower than the Debye length $\Delta x < \lambda_{\text{Debye}}$ for the simulation to be Physical. $v_{x,\text{min}}$ and $v_{x,\text{max}}$ should be chosen sufficiently large $|v_{x,\text{min}/\text{max}}| \gg v_{T_{e0}}$ in such a way that there is no plasma electrons outside the simulation velocity space during the whole simulation. The simulation velocity bin size should be chosen lower than the thermal electron velocity $\Delta v_x < v_{T_{e0}}$ and also sufficiently small to capture the desired Physics. The CFL stability condition (from the name of its finder R. Courant, K. Friedrichs and H. Lewy (R. Courant et al., 1928)) is implemented inside the code in such a way that the user just needs to specify in the input deck the scalar parameter $\text{cfl} < 1$ such that the normalized simulation time step reads

$$\Delta t_n = \text{cfl} \times F^n(\Delta x, \Delta v_x) < F^n(\Delta x, \Delta v_x) \quad (15)$$

at the time step $t_n = \sum_{m=1}^n \Delta t_m$ at time iteration n where $F^n(\Delta x, \Delta v_x)$ depends on the chosen numerical scheme.

For example, if one notes

$$\underline{f}_e^{n,i} = \frac{1}{\Delta x} \int_{x_{i-1/2}}^{x_{i+1/2}} \underline{f}_e(x, t_n) dx \quad (16)$$

the electron distribution function finite volume at the spatial location x_i located in between $x_{i-1/2} = x_i - \Delta x/2$ and $x_{i+1/2} = x_i + \Delta x/2$ and one considers the Lax-Wendroff method to compute the advection

$$\frac{\partial \underline{f}_e}{\partial t} + \underline{v}_x \frac{\partial \underline{f}_e}{\partial x} = 0 \quad (17)$$

of plasma electrons along the spatial x -axis in the phase-space, the numerical scheme reads

$$\left[\frac{\underline{f}_e^{n+1} - \underline{f}_e^n}{\Delta t_n} \right]^i + \underline{v}_x \left[\frac{\underline{F}_x^{i+1/2} - \underline{F}_x^{i-1/2}}{\Delta x} \right]^n = 0 \quad (18)$$

where the plasma electron fluxes across the volume sections located at $x_{i\pm 1/2}$ are given by

$$\underline{F}_x^{n,i+1/2} = \frac{\underline{f}_e^{n,i+1} + \underline{f}_e^{n,i}}{2} - \frac{\underline{v}_x \Delta t_n}{\Delta x} \frac{\underline{f}_e^{n,i+1} - \underline{f}_e^{n,i}}{2} \quad (19)$$

and

$$\underline{F}_x^{n,i-1/2} = \frac{\underline{f}_e^{n,i} + \underline{f}_e^{n,i-1}}{2} - \frac{\underline{v}_x \Delta t_n}{\Delta x} \frac{\underline{f}_e^{n,i} - \underline{f}_e^{n,i-1}}{2}. \quad (20)$$

According to the Taylor expansion of $\underline{f}_e^{n,i+i}$, $\underline{f}_e^{n,i-i}$ and $\underline{f}_e^{n+1,i}$ close to (x_i, t_n) up to the third order in space and time, one can check the Lax-Wendroff numerical consistency error is indeed of second order :

$$\begin{aligned} \underline{\epsilon}^{n,i} &= \left[\frac{\underline{f}_e^{n+1} - \underline{f}_e^n}{\Delta t_n} \right]^i + \underline{v}_x \left[\frac{\underline{F}_x^{i+1/2} - \underline{F}_x^{i-1/2}}{\Delta x} \right]^n - \left(\left. \frac{\partial \underline{f}_e}{\partial t} \right|^{n,i} + \underline{v}_x \left. \frac{\partial \underline{f}_e}{\partial x} \right|^{n,i} \right) \\ &= \frac{\Delta t_n^2}{6} \left. \frac{\partial^3 \underline{f}_e}{\partial t^3} \right|^{n,i} + \underline{v}_x \frac{\Delta x^2}{6} \left. \frac{\partial^3 \underline{f}_e}{\partial x^3} \right|^{n,i} + O(\Delta t_n^3 + \Delta x^3 + \Delta t_n \Delta x^2). \end{aligned} \quad (21)$$

By using the Von Neumann stability analysis, assuming periodic boundary conditions for simplicity and noting

$$\hat{\underline{f}}_e^n(k^p) = \frac{1}{N_x} \sum_{i=1}^{N_x} \underline{f}_e^{i,n} \exp(-i k^p x_i) \Leftrightarrow \underline{f}_e^{n,i} = \sum_{p=1}^{N_x} \hat{\underline{f}}_e^n(k^p) \exp(i k^p x_i) \quad (22)$$

with $\iota^2 = -1$, $N_x = 1 + (x_{\max} - x_{\min})/\Delta x$ the number of spatial grid points and $k^p = 2\pi(p-1)/(x_{\max} - x_{\min})$ the discrete Fourier mode, one gets by injecting Equation 22 in Equation 18

$$\frac{\hat{f}_e^{n+1}(k^p)}{\hat{f}_e^n(k^p)} = 1 - \frac{v_x \Delta t_n}{\Delta x} \iota \sin(k^p \Delta x) + \left(\frac{v_x \Delta t_n}{\Delta x} \right)^2 [\cos(k^p \Delta x) - 1] \quad (23)$$

for each term p of the series. It implies the numerical scheme is stable,

$$\text{meaning } \left| \frac{\hat{f}_e^{n+1}(k^p)}{\hat{f}_e^n(k^p)} \right| < 1, \text{ if } \Delta t_n < \frac{\Delta x}{v_x}. \quad (24)$$

Performing the same reasoning when discretizing also the velocity space $v_x^\ell = v_{x,\min} + (\ell - 1)\Delta v_x$ with $N_{v_x} = 1 + (v_{x,\max} - v_{x,\min})/\Delta v_x$ velocity grid points and considering in addition the advection term of plasma electrons along the v_x -axis in the velocity space for computing the Vlasov equation Equation 1 with each numerical scheme implemented in ESVM, one finds (sometimes empirically when it is too difficult analytically) that

$$F^n(\Delta x, \Delta v_x) = \frac{1/2}{\frac{\max_{\ell \in [1, N_{v_x}]} \{v_x^\ell\}}{\Delta x} + \frac{\max_{i \in [1, N_x]} \{E_x^{n,i}\}}{\Delta v_x}}. \quad (25)$$

is a sufficient CFL stability condition for all numerical schemes implemented in ESVM to be stable.

ESVM Plasma Physics academic case simulations

Four well-known Plasma Physics academic cases are provided with ESVM : 1) the emission of an electrostatic wakefield by a Gaussian electron; cf. Figure 1 2) the linear Landau damping of an electron plasma wave; cf. Figure 3, 3) the non-linear Landau damping of an electron plasma wave; cf. Figure 2 and 4) the two-stream instability of two counter-propagating symmetric Gaussian electron beams; cf. Figure 4.

For each academic case, an example of input deck is provided together with the corresponding simulation result plots that the code typically generates. For 1), 2) and 3), the simulation is initialized assuming a non-drifting collisionless plasma at Maxwell-Boltzmann equilibrium

$$\begin{cases} f_e^{(0)}(x, v_x, t = 0) &= \frac{Z n_i}{\sqrt{2\pi v_{Te_0}^2}} \exp\left[-\frac{v_x^2}{2v_{Te_0}^2}\right] \\ E_x^{(0)}(x, t = 0) &= 0 \end{cases} \quad (26)$$

that is perturbed : - with a small perturbation

$$\delta f_e(x, v_x, t = 0) = A \frac{Z n_i}{2\pi \delta x \delta v} \exp\left[-\frac{(x - x_d)^2}{2\delta x^2}\right] \exp\left[-\frac{(v_x - v_d)^2}{2\delta v^2}\right], \quad (27)$$

consisting in a Gaussian electron located at $x_d = x_{\min} + (x_{\max} - x_{\min})/8$ with a standard deviation $\delta x = \lambda_{\text{Debye}}/4$ and drifting at a velocity v_d with a standard deviation $\delta v = v_{Te_0}/40$ at the simulation start $t = 0$ for 1), and - with a small perturbation consisting in a small amplitude electron plasma wave

$$\delta E_x(x, t < \delta t) = A \frac{m_e \omega_p v_{Te_0}}{e} \sin(\omega_0 t - kx) \quad (28)$$

156 propagating during a short time interval $\delta t = 6\pi/\omega_0$ after the simulation start $t = 0$ for 2)
157 and 3).

158 Only the perturbation amplitudes $A < 1$ for 1), 2) and 3), the perturbation drift velocity
159 $v_d > v_{Te0}$ for 1) and the perturbation temporal and spatial angular frequencies ω_0 and k for
160 2) and 3) should be modified by the user when filling the input-deck in such a way that

$$\begin{cases} f_e(x, v_x, t) = f_e^{(0)}(x, v_x, t) + \delta f_e(x, v_x, t) \\ E_x(x, t) = E_x^{(0)}(x, t) + \delta E_x(x, t) \end{cases} \quad \text{with } |\delta f_e(x, v_x, t)| \ll f_e^{(0)}(x, v_x, t) \quad (29)$$

161 keeps being respected during the linear stage of the simulation. Except for non-linear Plasma
162 Physics processes such as 3) for which the non-linear theory should be considered, the method-
163 ology that can be used to check any ESVM simulation results is always the same. Only
164 analytical estimates used to check the ESVM simulation results of the provided academic
165 case 4) are consequently detailed here in order to highlight it. The user can check the
166 provided academic case simulation results 1), 2) and 3) by directly comparing the ESVM sim-
167 ulation results with the analytical estimates provided in (Decyk, 1987) (available at <https://picksc.idre.ucla.edu/wp-content/uploads/2015/04/DecykKyiv1987.pdf>) and in the refer-
168 ence textbooks (Landau & Lifshitz, 1981) and (Sagdeev & Galeev, 1969), respectively.
169

170 The provided Plasma Physics academic case 4) is initialized assuming two counter-propagating
171 homogeneous Gaussian electron beams 'e, +' and 'e, -' of exactly opposite drift velocity $\pm v_d$
172 with same standard velocity deviation v_{Te0}

$$f_e^{(0)}(x, v_x, t) = f_{e,+}^{(0)}(x, v_x, t) + f_{e,-}^{(0)}(x, v_x, t) \quad (30)$$

173 with

$$f_{e,\pm}^{(0)}(x, v_x, t) = \frac{Zn_i/2}{\sqrt{2\pi}v_{Te0}^2} \exp\left[-\frac{(v_x \mp v_d)^2}{2v_{Te0}^2}\right] \quad (31)$$

174 that is a solution of the Vlasov Equation Equation 1 and that doesn't produce any electrostatic
175 fields

$$E_x^{(0)}(x, t) = 0 \quad (32)$$

176 according to Maxwell-Gauss Equation Equation 2. If one computes the Vlasov-Maxwell set
177 of Equations {Equation 1, Equation 2} exactly, initializing it with the two-stream equilibrium
178 distribution function Equation 30 without any perturbation, the counter-propagating elec-
179 tron beams would continue their propagation through the immobile plasma ions without any
180 modification. In order to observe the two-stream instability,

$$f_e(x, v_x, t = 0) = f_e^{(0)}(x, v_x, t = 0) + \delta f_e(x, v_x, t = 0), \quad (33)$$

181 is initialized instead by adding a small perturbation

$$\delta f_e(x, v_x, t = 0) = \delta f_{e,+}(x, v_x, t = 0) + \delta f_{e,-}(x, v_x, t = 0) \quad (34)$$

182 on each beam of the form

$$\delta f_{e,\pm}(x, v_x, t = 0) = \pm A \sin(k_1 x) f_{e,\pm}^{(0)}(x, v_x, t = 0) \quad (35)$$

183 at the simulation start $t = 0$ with $A = 0.1$, $k_1 = 2\pi/L_x$ (parameter k in the input-deck)
184 where $L_x = x_{\max} - x_{\min}$ can be modified by the user in the input-deck.

185 In order to get analytical estimates of growing plasma electron density and mean velocity and
186 electrostatic fields in this ESVM simulation, one can linearize the Vlasov equation Equation 1
187 and the self-consistent Maxwell-Gauss equation Equation 2 computed by ESVM assuming the

188 perturbation Equation 34 remains small compared to the equilibrium distribution Equation 30
189 during the simulation. They read

$$\frac{\partial \delta f_e}{\partial t} + \frac{\partial}{\partial x} (v_x \delta f_e) - \frac{e}{m_e} \frac{df_e^{(0)}}{dv_x} \delta E_x = 0 \quad (36)$$

190 and

$$\frac{\partial \delta E_x}{\partial x} = -4\pi e \int_{-\infty}^{\infty} \delta f_e dv_x, \quad (37)$$

191 up to the first order. Considering periodic boundary conditions, we may use a one-sided
192 Fourier transformation in time (thus equivalent to a Laplace transform) and a Fourier series
193 expansion in space for such a L_x -periodic initial condition problem. We will note

$$\widehat{X}_p(t) = \frac{1}{L_x} \int_0^{L_x} X(x, t) \exp(+\iota k_p x) dx \Leftrightarrow X(x, t) = \sum_{p=-\infty}^{\infty} \widehat{X}_p(t) \exp(-\iota k_p x) \quad (38)$$

194 with $\forall p \in \mathbb{Z}, k_p = 2\pi p/L_x$ and

$$\begin{aligned} \widehat{\widehat{X}}_p^{(+)}(\omega) &= \int_0^{\infty} dt \widehat{X}_p(t) \exp(-\iota \omega t) \\ &= \int_0^{\infty} dt \int_0^{L_x} \frac{dx}{L_x} X(x, t) \exp[-\iota(\omega t - k_p x)] \\ \Leftrightarrow X(x, t) &= \int_{\iota R - \infty}^{\iota R + \infty} \frac{d\omega}{2\pi} \sum_{p=-\infty}^{\infty} \widehat{\widehat{X}}_p^{(+)}(\omega) \exp[+\iota(\omega t - k_p x)] \end{aligned} \quad (39)$$

195 where the integral in the complex ω -plane is taken along a straight line $\omega = \iota R$. By multiplying
196 Equation 36 and Equation 37 by $\exp[-\iota(\omega t - k_p x)]/L_x$ and by integrating them from $x =$
197 $-\infty$ to $x = \infty$ and from $t = 0$ to $t = \infty$, we obtain respectively

$$\widehat{\widehat{\delta f}}_{e,p}^{(+)} = \frac{1}{\iota(\omega - k_p v_x)} \left[\widehat{\delta f}_{e,p}(v_x, t=0) + \frac{e}{m_e} \frac{df_e^{(0)}}{dv_x} \widehat{\widehat{E}}_{x,p}^{(+)} \right] \quad (40)$$

198 with

$$\widehat{\delta f}_{e,p}(v_x, t=0) = \alpha_p A \frac{Z n_i / 2}{\sqrt{2\pi v_{Te_0}^2}} \left\{ \exp\left[-\frac{(v_x - v_d)^2}{2v_{Te_0}^2}\right] - \exp\left[-\frac{(v_x + v_d)^2}{2v_{Te_0}^2}\right] \right\} \quad (41)$$

199 where

$$\alpha_p = \begin{cases} \mp 1/2\iota & \text{if } p = \pm 1 \\ 0 & \text{else} \end{cases} \quad (42)$$

200 and

$$\widehat{\widehat{E}}_{x,p}^{(+)} = \frac{4\pi e}{\iota k_p} \int_{-\infty}^{\infty} \widehat{\delta f}_{e,p}^{(+)}(\omega, v_x) dv_x. \quad (43)$$

201 Injecting Equation 40 in Equation 43, we obtain the Fourier components of the electrostatic
202 field Laplace transform

$$\begin{aligned} \widehat{\widehat{\delta E}}_{x,p}^{(+)}(\omega) &= \frac{4\pi e}{k_p^2 \epsilon(\omega, k_p)} \int_{-\infty}^{\infty} \frac{\widehat{\delta f}_{e,p}(v_x, t=0)}{v_x - \omega/k_p} dv_x \\ &= \alpha_p \frac{A}{2\sqrt{2}} \frac{m_e v_{Te_0}}{e} \frac{\mathcal{Z}\left(\frac{\omega/k_p - v_d}{v_{Te_0} \sqrt{2}}\right) - \mathcal{Z}\left(\frac{\omega/k_p + v_d}{v_{Te_0} \sqrt{2}}\right)}{\epsilon(\omega, k_p) (k_p \lambda_{\text{Debye}})^2} \end{aligned} \quad (44)$$

203 where the plasma electrical permittivity reads

$$\begin{aligned}\epsilon(\omega, k) &= 1 - \frac{4\pi e^2}{m_e k^2} \int_{-\infty}^{\infty} \frac{1}{v_x - \omega/k} \frac{df_e^{(0)}}{dv_x} dv_x \\ &= 1 + \frac{1}{(k\lambda_{\text{Debye}})^2} \left\{ 1 + \frac{1}{2} \left[F\left(\frac{\omega/k - v_d}{v_{Te_0}\sqrt{2}}\right) + F\left(\frac{\omega/k + v_d}{v_{Te_0}\sqrt{2}}\right) \right] \right\}\end{aligned}\quad (45)$$

204 depending on the plasma dispersion function (Fried & Conte, 1961)

$$F(\zeta) = \zeta \mathcal{Z}(\zeta) \quad \text{and} \quad \mathcal{Z}(\zeta) = \frac{1}{\sqrt{\pi}} \int_{-\infty}^{\infty} \frac{\exp(-z^2)}{z - \zeta} dz. \quad (46)$$

205 Since $v_d \gg v_{Te_0}$ in this ESVM simulation, we have the condition

$$\left| \frac{\omega}{k_p} \pm v_d \right| \gg v_{Te_0} \sqrt{2} \quad (47)$$

206 that is fulfilled for any given spatial frequency mode k_p and one thus may use the asymptotic
207 limit

$$F(\zeta) \underset{|\zeta| \gg 1}{=} i\zeta\sqrt{\pi} \exp(-\zeta^2) - 1 - \frac{1}{2\zeta^2} - \frac{3}{4\zeta^4} + O\left(\frac{1}{\zeta^6}\right) \quad (48)$$

208 that leads to the simpler dispersion relation

$$\epsilon(\omega, k) \underset{v_d \gg v_{Te_0}}{=} 1 - \frac{\omega_p^2}{2} \left[\frac{1}{(\omega - kv_d)^2} + \frac{1}{(\omega + kv_d)^2} \right] = 0 \quad (49)$$

209 retaining only the main term in the series expansion of the dispersion function [Equation 46](#)
210 up to the second order [Equation 48](#). In this limit, the dispersion relation [Equation 49](#) provides
211 four pure real solutions $\{\omega_1(k), \omega_2(k), \omega_3(k), \omega_4(k)\} \in \mathbb{R}^4$ for wavenumber k greater
212 or equal than the critical wavenumber ω_p/v_d . It means that the two counter-propagating
213 electron beams remain stable on space scales smaller than $2\pi v_d/\omega_p$. However, in the case
214 where $k_p < \omega_p/v_d$ considered here, one finds in addition to the two real poles

$$\omega_{1/2}\left(k < \frac{\omega_p}{v_d}\right) = \pm\omega_0(k) \quad (50)$$

215 where

$$\omega_0(k) = \omega_p \sqrt{\left(\frac{kv_d}{\omega_p}\right)^2 + \frac{1}{2} \left(1 + \sqrt{1 + 8\left(\frac{kv_d}{\omega_p}\right)^2}\right)} \underset{kv_d \ll \omega_p}{\sim} \omega_p, \quad (51)$$

216 two another pure imaginary conjugate poles

$$\omega_{3/4}(k < k_c) = \pm i\delta(k). \quad (52)$$

217 It means that the two counter-propagating electron beams streaming throught the immobile
218 plasma ions are unstable on space scales greater than $2\pi v_d/\omega_p$ and that this two-stream
219 instability grows exponentially at the rate

$$\delta(k) = \omega_p \sqrt{\frac{1}{2} \left(\sqrt{1 + 8\left(\frac{kv_d}{\omega_p}\right)^2} - 1 \right) - \left(\frac{kv_d}{\omega_p}\right)^2} \underset{kv_d \ll \omega_p}{\sim} |k| v_d. \quad (53)$$

220 The stable electron plasma waves angular frequency [Equation 51](#) and the two stream instability
221 growth rate [Equation 53](#) are plotted in [Figure 5](#) as a function of the angular spatial frequency
222 mode k . Retaining the main terms in the series expansions of \mathcal{Z} up to the second order

in Equation 44 according to Equation 48, the Fourier components of the electrostatic field Laplace transform simplify into

$$\widehat{\delta E}_{x,p}^{(+)}(\omega) \underset{v_d \gg v_{Te_0}}{\sim} -\alpha_p A \frac{m_e v_d}{e} \frac{\omega_p^2}{\epsilon(\omega, k_p) (\omega - k_p v_d) (\omega + k_p v_d)}. \quad (54)$$

The poles of the Fourier components of the electrostatic fields Equation 54 are thus $\pm k_p v_d$ plus the ones of the plasma electrical permittivity Equation 49 given by Equations 50 and Equation 52. We can now determine the time dependence of the spatial Fourier components of the growing electrostatic field

$$\widehat{\delta E}_{x,p}(t) = \frac{1}{2\pi} \int_{\iota R - \infty}^{\iota R + \infty} \widehat{\delta E}_{x,p}^{(+)}(\omega) \exp(+\iota \omega t) d\omega \quad (55)$$

by using the residue theorem with the contour illustrated in Figure 6 in order to evaluate the Cauchy principal value of this integral : since the function to integrate in Equation 55 is an analytic function of ω defined in the whole complex plane, we moved the contour of integration usually taken slightly above the real axis into the lower half-plane sufficiently far beneath the pole $-\iota \delta$ and passing round this pole and round the other poles lying above it in such a way that it doesn't cross any of the poles of the function. We thus obtain

$$\begin{aligned} \widehat{\delta E}_{x,p}(t) &= A E_0 \alpha_p \frac{\omega_p}{\delta(k_p)} \frac{\delta(k_p)^2 + (k_p v_d)^2}{\delta(k_p)^2 + \omega_0(k_p)^2} \sinh[\delta(k_p) t] \\ &+ A \frac{E_0}{2} \alpha_p \frac{\omega_p}{\omega_0(k_p)} \frac{\omega_0(k_p)^2 - (k_p v_d)^2}{\delta(k_p)^2 + \omega_0(k_p)^2} \sin[\omega_0(k_p) t] \end{aligned} \quad (56)$$

with

$$E_0 = \frac{m_e v_d \omega_p}{e} \quad (57)$$

that finally gives according to the Fourier series expansion Equation 38

$$\begin{aligned} \delta E_x(x, t) &= A E_0 \frac{\omega_p}{\delta(k_1)} \frac{\delta(k_1)^2 + (k_1 v_d)^2}{\delta(k_1)^2 + \omega_0(k_1)^2} \sinh[\delta(k_1) t] \sin(k_1 x) \\ &+ A \frac{E_0}{2} \frac{\omega_p}{\omega_0(k_1)} \frac{\omega_0(k_1)^2 - (k_1 v_d)^2}{\delta(k_1)^2 + \omega_0(k_1)^2} \sin[\omega_0(k_1) t] \sin(k_1 x). \end{aligned} \quad (58)$$

Knowing the electrostatic field Equation 58, one may also deduce the perturbed distribution function according to Equation 36. It reads

$$\begin{aligned} \delta f_e(x, v_x, t) &= \delta f_e(x, v_x, t=0) + \frac{e}{m_e} \frac{df_e^{(0)}}{dv_x}(v_x) \int_0^t \delta E_x[x + v_x(\tau - t), \tau] d\tau \\ &= f_{e,+}^{(0)}(v_x) \left[+A \sin(k_1 x) + \frac{v_d - v_x}{v_{Te_0}^2} \frac{e}{m_e} \int_0^t \delta E_x[x + v_x(\tau - t), \tau] d\tau \right] \\ &+ f_{e,-}^{(0)}(v_x) \left[-A \sin(k_1 x) - \frac{v_d + v_x}{v_{Te_0}^2} \frac{e}{m_e} \int_0^t \delta E_x[x + v_x(\tau - t), \tau] d\tau \right]. \end{aligned} \quad (59)$$

In the limit $k_p v_d \ll \omega_p$, they simplify into

$$\delta E_x(x, t) \underset{k_1 v_d \ll \omega_p}{\sim} A \frac{E_0}{2} \left[\sin(\omega_p t) + 4 \frac{k_1 v_d}{\omega_p} \sinh(k_1 v_d t) \right] \sin(k_1 x) \quad (60)$$

240 and

$$\begin{aligned}
 & \sim_{k_1 v_d \ll \omega_p} A \frac{v_d}{1 - \left(\frac{k_1 v_x}{\omega_p}\right)^2} \left\{ \frac{e}{m_e} \int_0^t \delta E_x [x + v_x (\tau - t), \tau] d\tau \right. \\
 & + \left. A \frac{v_d}{1 + \left(\frac{v_x}{v_d}\right)^2} \left\{ -\frac{v_x}{v_d} \sinh(k_1 v_d t) \cos(k_1 x) + [\cosh(k_1 v_d t) - 1] \sin(k_1 x) \right\} \right\}.
 \end{aligned} \quad (61)$$

241 We thus deduce in this limit

$$\begin{aligned}
 \delta n_e(x, t) &= \int_{-\infty}^{\infty} \delta f_e(x, v_x, t) dv_x \\
 &\sim_{k_1 v_d \ll \omega_p} -\frac{A}{2} Z n_i \frac{k_1 v_d}{\omega_p} \left[\sin(\omega_p t) + 4 \frac{k_1 v_d}{\omega_p} \sinh(k_1 v_d t) \right] \cos(k_1 x)
 \end{aligned} \quad (62)$$

242 and

$$\begin{aligned}
 \delta v_e(x, t) &= \frac{1}{Z n_i} \int_{-\infty}^{\infty} v_x \delta f_e(x, v_x, t) dv_x \\
 &\sim_{k_1 v_d \ll \omega_p} -\frac{A}{2} v_d \left[(\cos(\omega_p t) - 1) + \left(2 \frac{k_1 v_d}{\omega_p}\right)^2 (\cosh(k_1 v_d t) - 1) \right] \sin(k_1 x).
 \end{aligned} \quad (63)$$

243 The first term in the square brackets

$$\begin{cases} \delta n_{\text{osc}}(x, t) & \sim_{k_1 v_d \ll \omega_p} -\frac{A}{2} Z n_i \frac{k_1 v_d}{\omega_p} \sin(\omega_p t) \cos(k_1 x) \\ \delta v_{\text{osc}}(x, t) & \sim_{k_1 v_d \ll \omega_p} -\frac{A}{2} v_d (\cos(\omega_p t) - 1) \sin(k_1 x) \\ \delta E_{\text{osc}}(x, t) & \sim_{k_1 v_d \ll \omega_p} \frac{A}{2} E_0 \sin(\omega_p t) \sin(k_1 x) \end{cases} \quad (64)$$

244 corresponds to space-charge oscillations of stationary electrostatic plasma waves excited by
 245 the perturbation imposed on each electron beam. We are rather interested here in the second
 246 term in the square brackets

$$\begin{cases} \delta n_{\text{ins}}(x, t) & \sim_{k_1 v_d \ll \omega_p} -2A Z n_i \left(\frac{k_1 v_d}{\omega_p}\right)^2 \sinh(k_1 v_d t) \cos(k_1 x) \\ \delta v_{\text{ins}}(x, t) & \sim_{k_1 v_d \ll \omega_p} -2A v_d \left(\frac{k_1 v_d}{\omega_p}\right)^2 (\cosh(k_1 v_d t) - 1) \sin(k_1 x) \\ \delta E_{\text{ins}}(x, t) & \sim_{k_1 v_d \ll \omega_p} 2A E_0 \frac{k_1 v_d}{\omega_p} \sinh(k_1 v_d t) \sin(k_1 x) \end{cases} \quad (65)$$

247 corresponding to the exponentially growing electrostatic field due to the two-stream instabil-
 248 ity. These latter growing electron density, current density and electrostatic field perturbations
 249 Equation 65 can directly be compared with the ESVM simulation result. One can also check
 250 that if $A = 0$, all quantities cancel. That confirms that, contrary to PIC codes, the two
 251 counter-propagating electron beams would continue their propagation without any modifica-
 252 tion if we do not impose an initial perturbation on which the instability will grow in ESVM.
 253 Finally, one can estimate the trajectories (x_ℓ, v_ℓ) of one beam electron $\ell \in [1, N_e]$ with an
 254 arbitrary initial velocity $v_\ell(t=0) = v_0$ in the beam velocity distribution function and an
 255 initial position $x_\ell(t=0) = x_0$ close to $x = 0$ such that $k_1 x_0 \ll 1$. At the early stage of
 256 the instability, the growing electrostatic field component δE_{ins} is small compared to the sta-
 257 tionary plasma wave δE_{osc} that oscillates in time at the Langmuir electron angular frequency

258 ω_p . On such time scale $\omega_p t \sim 1$, the beam electrons are consequently mainly affected by this
259 electrostatic field component

$$m_e \frac{dv_\ell}{dt} = -e\delta E_{\text{osc}}(x_\ell(t), t) \quad (66)$$

260 and their trajectory is thus given by

$$\frac{d^2 x_\ell}{dt^2} + \omega_p^2 \left(\frac{A k_1 v_d}{2 \omega_p} \right) \sin(\omega_p t) x_\ell(t) = 0, \quad (67)$$

261 assuming that $k_1 x_\ell(t) \ll 1$ remains valid at every time $t > 0$ if it is valid at $t = 0$ such that
262 $\forall t, \sin[k_1 x_\ell(t)] \sim k_1 x_\ell(t)$. Recognizing the Mathieu Equation

$$\frac{d^2 x_\ell}{du^2} + [a - 2q \cos(2u)] x_\ell(u) = 0 \quad (68)$$

263 with $a = 0$ and $q = -Ak_1 v_d / \omega_p$ by doing the change of variable $u(t) = (-\pi/4) + (\omega_p t/2)$,
264 we deduce

$$k_1 x_\ell(t) = k_1 x_c c_{e,0}[q, u(t)] + k_1 x_s s_{e,0}[q, u(t)] \quad (69)$$

265 and

$$v_\ell(t) = \frac{v_d}{2} \frac{\omega_p}{k_1 v_d} \{ k_1 x_c c'_{e,0}[q, u(t)] + k_1 x_s s'_{e,0}[q, u(t)] \} \quad (70)$$

266 with

$$\begin{cases} k_1 x_c = + \frac{s'_{e,0}(q, -\pi/4) k_1 x_0 - s_{e,0}(q, -\pi/4) (2k_1 v_d / \omega_p) (v_0 / v_d)}{c_{e,0}(q, -\pi/4) s'_{e,0}(q, -\pi/4) - c'_{e,0}(q, -\pi/4) s_{e,0}(q, -\pi/4)} \\ k_1 x_s = - \frac{c'_{e,0}(q, -\pi/4) k_1 x_0 - c_{e,0}(q, -\pi/4) (2k_1 v_d / \omega_p) (v_0 / v_d)}{c_{e,0}(q, -\pi/4) s'_{e,0}(q, -\pi/4) - c'_{e,0}(q, -\pi/4) s_{e,0}(q, -\pi/4)} \end{cases}, \quad (71)$$

267 accounting for the initial conditions at $t = 0$. Here, $c_{e,a}(q, u)$ and $s_{e,a}(q, u)$ are respectively
268 the even and odd solutions of Mathieu Equation Equation 68 and $c'_{e,a}(q, u)$ and $s'_{e,a}(q, u)$
269 their first order derivatives. According to Equation 69 and Equation 70, the beam electron
270 trajectories in space are only slightly modified compared to their ballistic initial trajectory
271 $x_0 + v_0 t$ with a velocity that oscillates around their initial value v_0 with amplitudes slightly
272 increasing with time. As a consequence, each beam velocity dispersion slightly increases with
273 its propagation distance until the growing component of the electrostatic field δE_{ins} becomes
274 greater than δE_{osc} . When this occurs, the equation of motion

$$m_e \frac{dv_\ell}{dt} = -e\delta E_{\text{ins}}(x_\ell(t), t) \quad (72)$$

275 gives

$$\frac{1}{2} \left(\frac{v_\ell(t)}{v_d} \right)^2 - \frac{1}{2} \left(\frac{v_0}{v_d} \right)^2 = -2Ak_1 \int_0^t v_\ell(t) \sin[k_1 x_\ell(t)] \sinh(k_1 v_d t) dt \quad (73)$$

276 and

$$\frac{d^2 x_\ell}{dt^2} + 2k_1 v_d^2 \sinh(k_1 v_d t) \sin[k_1 x_\ell(t)] = 0. \quad (74)$$

277 The energy conservation Equation Equation 73 shows that, at the early stage of the instability,
278 electrons having a positive velocity $v_\ell(t) > 0$ at a location $0 < x_\ell(t) < L_x/2$ as well as
279 electrons having a negative velocity $v_\ell(t) < 0$ at a location $-L_x/2 < x_\ell(t) < 0$ are losing
280 energy contrary to electrons having a negative velocity $v_\ell(t) < 0$ at a location $0 < x_\ell(t) < L_x/2$
281 or electrons having a positive velocity $v_\ell(t) > 0$ at a location $-L_x/2 < x_\ell(t) < 0$
282 that are earning energy. In order to determine such an electron trajectory according to its
283 equation of motion Equation 74, one can assume in addition that $k_1 x_\ell(t) \ll 1$ remains valid
284 at every time $t > 0$ if it is valid at $t = 0$ such that $\forall t, \sin[k_1 x_\ell(t)] \sim k_1 x_\ell(t)$ and consider

time scales of the order of electrostatic plasma oscillations ω_p^{-1} so that we may consider $\sinh(k_1 v_d t) \sim \exp(k_1 v_d t)/2$. In this case, Equation 74 simplifies into

$$\frac{d^2 x_\ell}{dt^2} + (k_1 v_d)^2 \exp(k_1 v_d t) x_\ell(t) = 0. \quad (75)$$

Recognizing the differential Bessel Equation by doing the change of variable $v(t) = \exp(k_1 v_d t)$

$$\frac{d^2 x_\ell}{dv^2} + \frac{1}{v} \frac{dx_\ell}{dv} + \frac{1}{v} x_\ell(v) = 0, \quad (76)$$

the beam electron trajectories can be found readily. They read

$$k_1 x_\ell(t) = k_1 x_J J_0(2\sqrt{v(t)}) + k_1 x_Y Y_0(2\sqrt{v(t)}) \quad (77)$$

and

$$v_\ell(t) = -v_d \left[k_1 x_J J_1(2\sqrt{v(t)}) + k_1 x_Y Y_1(2\sqrt{v(t)}) \right] \sqrt{v(t)} \quad (78)$$

with

$$\begin{cases} k_1 x_J &= + \frac{Y_1(2) k_1 x_0 + Y_0(2) (v_0/v_d)}{J_0(2) Y_1(2) - J_1(2) Y_0(2)} \\ k_1 x_Y &= - \frac{J_1(2) k_1 x_0 + J_0(2) (v_0/v_d)}{J_0(2) Y_1(2) - J_1(2) Y_0(2)} \end{cases}, \quad (79)$$

accounting for the initial conditions at $t = 0$. Here, J_μ and Y_μ are the Bessel functions of the first and second kind of order μ respectively. Some of these beam electron orbits are plotted in Figure 7. We can see that the beam electrons are looping around the phase-space center $(x, v) = (0, 0)$ with a velocity amplitude increasing with their initial spatial distance from $x = 0$ in agreement with the ESVM simulation Figure 4.

ESVM Perspectives

It is planned in a near future to : - provide another Plasma Physics academic simulation about one BGK (from the name of its finder I. B. Bernstein, J. M. Greene and M. D. Kruskal) non linear solution (Bernstein et al., 1957) - provide a second Plasma Physics academic simulation about Plasma wave echo (Gould et al., 1967) - implement non-equally spaced phase-space cells - implement high order Weighted Essentially Non-Oscillatory (WENO) advection schemes (Liu et al., 1994) - compute the plasma ion Vlasov equation to allow for the ions to be mobile - extend the code to relativistic electromagnetic 2D-2V and 1D-3V phase-space electromagnetic plasma simulations : ESVM \Rightarrow EMVM (open source ElectroMagnetic Vlasov-Maxwell code) - store the simulation results in hdf5 files instead of text files - implement its MPI parallelization - implement its vectorization - implement the Perfectly Matched Layer (PML) technique (Berenger, 1994) to absorb the electromagnetic fields at the spatial simulation box boundaries - implement a relativistic BGK (from the name of its finder P. L. Bhatnagar, E. P. Gross and M. Krook) collision operator (Bhatnagar et al., 1954) - implement the Belyaev-Budker relativistic collision operator (Belaiev & Budker, 1956) using the Braams-Karney relativistic extension of Rosenbluth potentials (Braams & Karney, 1987) : EMVM \Rightarrow EMVFPBBM (open source ElectroMagnetic Vlasov-Fokker-Planck-Belyaev-Budker-Maxwell code) - deploy the code to GPU architectures.

315 Figures

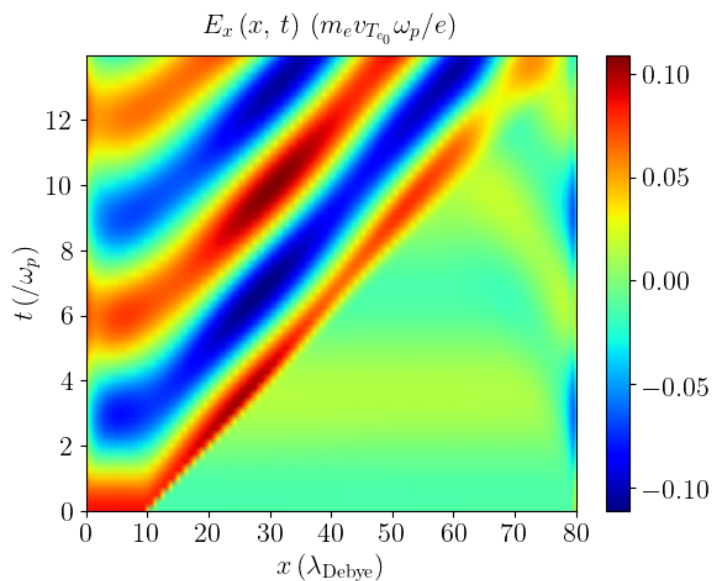


Figure 1: Electrostatic wakefield test case : Electrostatic wakefield $E_x(x, t)$ emitted by a Gaussian electron propagating in a collisionless plasma at Maxwell-Boltzmann equilibrium Equation 26 and initialized according to Equation 27 with $A = 0.1$ and $v_d = 5$.

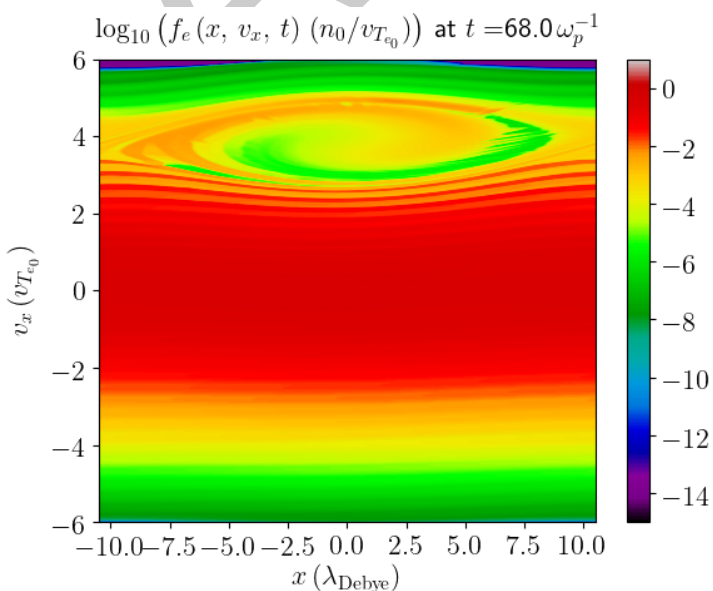


Figure 2: Non Linear Landau damping test case : Plasma electrons phase-space $f_e(x, v_x, t = 68)$ in the non-linear Landau damping of the electron plasma wave propagating in the collisionless plasma at Maxwell-Boltzmann equilibrium Equation 26 and and initialized according to Equation 28 with $A = 10^{-1}$, $\underline{k} = 0.29919930034$ and $\underline{\omega}_0 = 1.18$.

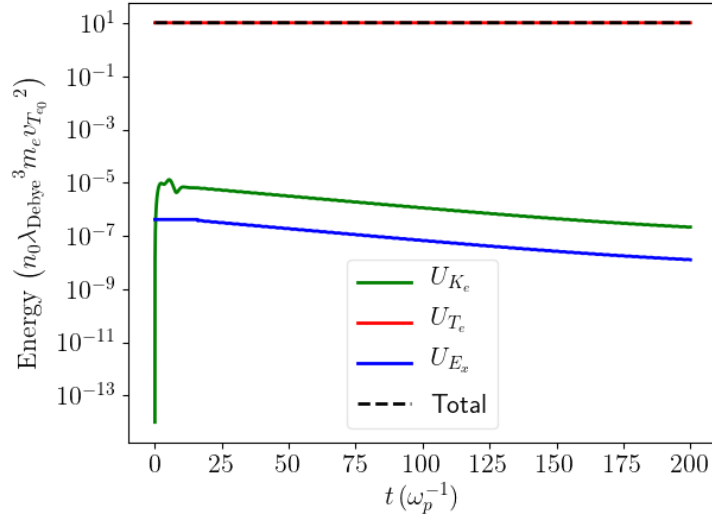


Figure 3: Linear Landau damping test case : Total electrostatic field energy and plasma electrons kinetic energy time evolution of the linearly Landau damped electron plasma wave propagating in the collisionless plasma at Maxwell-Boltzmann equilibrium Equation 26 and initialized according to Equation 28 with $A = 10^{-3}$, $\underline{k} = 0.29919930034$ and $\underline{\omega}_0 = 1.18$.

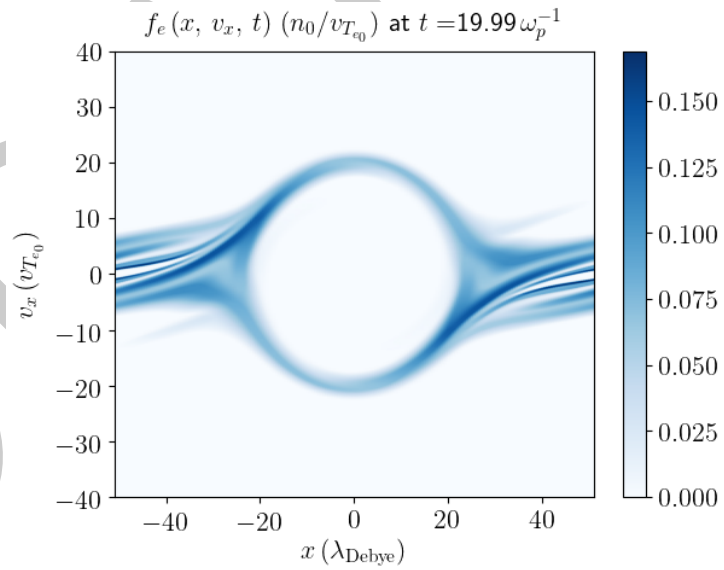


Figure 4: Two stream instability test case : Plasma electrons phase-space $f_e(x, v_x, t = 19.99)$ in the two-stream instability of two counter-propagating electron beams initialized according to Equation 33 with $A = 10^{-1}$, $\underline{k} = 0.06159985595$ ($x_{\min} = -x_{\max} = 51$) and $\underline{v}_d = 10$.

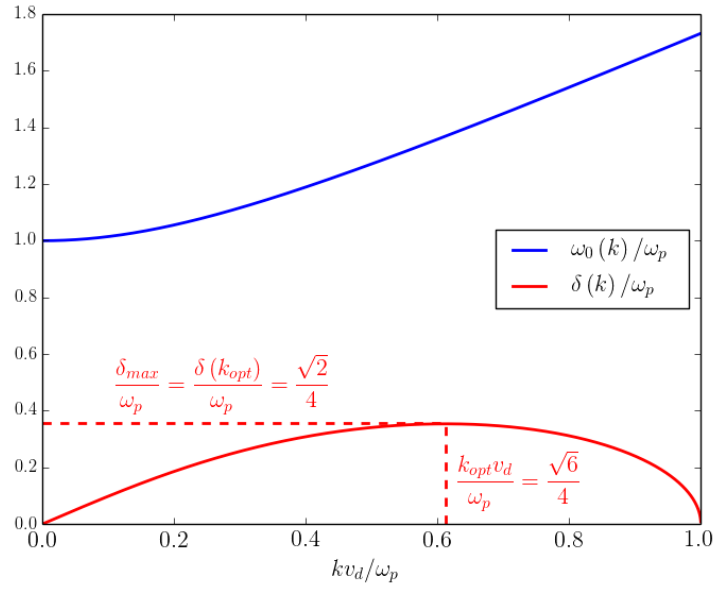


Figure 5: Two stream instability test case : Stationary electron plasma waves angular frequency Equation 51 seeded by the perturbation Equation 34 and the two-stream instability growth rate Equation 53 as a function of the spatial angular frequency mode k .

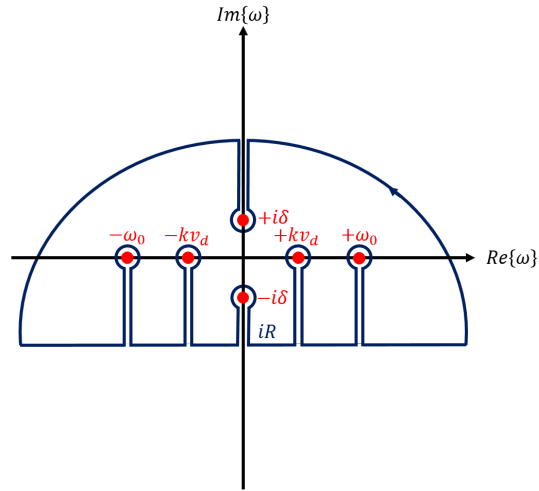


Figure 6: Two stream instability test case : Integration contour used to evaluate the the Cauchy principal value of the integral Equation 55.

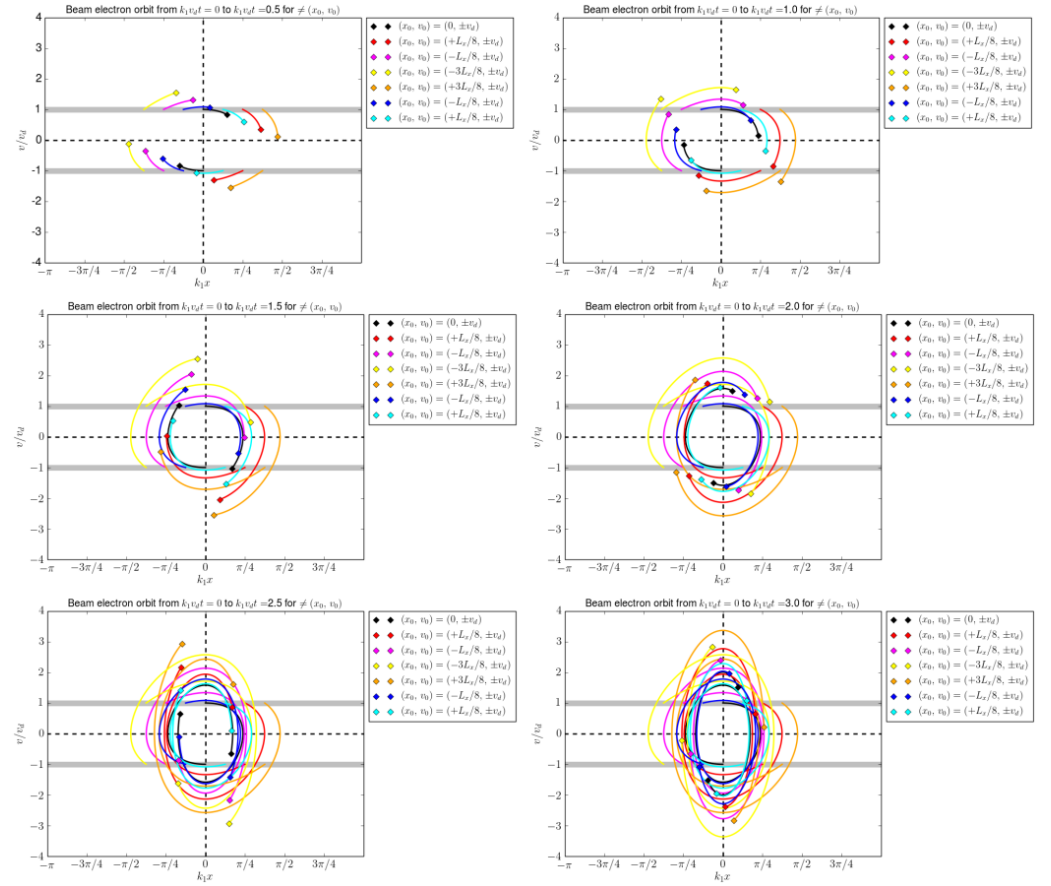


Figure 7: Two stream instability test case : Some beam electron orbits according to analytical estimates Equation 77 and Equation 78.

References

- Beam, R. M., & Warming, R. F. (1976). An implicit finite-difference algorithm for hyperbolic systems in conservation-law form. *Journal of Computational Physics*, 22(1), 87–110. [https://doi.org/10.1016/0021-9991\(76\)90110-8](https://doi.org/10.1016/0021-9991(76)90110-8)
- Belaiev, S. T., & Budker, G. I. (1956). *Dokl. Akad. Nauk SSSR*, 107.
- Berenger, J.-P. (1994). A perfectly matched layer for the absorption of electromagnetic waves. *Journal of Computational Physics*, 114(2), 185–200. <https://doi.org/10.1006/jcph.1994.1159>
- Bernstein, I. B., Greene, J. M., & Kruskal, M. D. (1957). Exact nonlinear plasma oscillations. *Phys. Rev.*, 108, 546–550. <https://doi.org/10.1103/PhysRev.108.546>
- Bhatnagar, P. L., Gross, E. P., & Krook, M. (1954). A model for collision processes in gases. I. Small amplitude processes in charged and neutral one-component systems. *Phys. Rev.*, 94, 511–525. <https://doi.org/10.1103/PhysRev.94.511>
- Braams, B. J., & Karney, C. F. F. (1987). Differential form of the collision integral for a relativistic plasma. *Phys. Rev. Lett.*, 59, 1817–1820. <https://doi.org/10.1103/PhysRevLett.59.1817>
- Courant, R., Friedrichs, K., & Lewy, H. (1928). Über die partiellen differenzengleichungen der mathematischen. *Physik. Math. Ann.*, 100, 32–74. <https://doi.org/10.1007/BF01532856>

- 334 [10.1007/BF01448839](https://doi.org/10.1007/BF01448839)
- 335 Courant, R., Isaacson, E., & Rees, M. (1952). On the solution of nonlinear hyperbolic differ-
 336 ential equations by finite differences. *Communications on Pure and Applied Mathematics*,
 337 5(3), 243–255. <https://doi.org/https://doi.org/10.1002/cpa.3160050303>
- 338 Crouseilles, N., & Filbet, F. (2004). Numerical approximation of collisional plasmas by high or-
 339 der methods. *Journal of Computational Physics*, 201(2), 546–572. <https://doi.org/https://doi.org/10.1016/j.jcp.2004.06.007>
- 340
- 341 Dawson, J. (1962). One-dimensional plasma model. *The Physics of Fluids*, 5(4), 445–459.
 342 <https://doi.org/https://doi.org/10.1063/1.1706638>
- 343 de Buyl, P. (2014). The vmf90 program for the numerical resolution of the vlasov equa-
 344 tion for mean-field systems. *Computer Physics Communications*, 185(6), 1822–1827.
 345 <https://doi.org/https://doi.org/10.1016/j.cpc.2014.03.004>
- 346 Decyk, V. K. (1987). Simulation of microscopic processes in plasma. *Proc. 1987 International*
 347 *Conference on Plasma Physics, Kiev, USSR, April 1987, Ed. A G Sitenko [World Scientific,*
 348 *Singapore, 1987] Vol. II, p. 1075.*
- 349 Derouillat, J., Beck, A., Pérez, F., Vinci, T., Chiaramello, M., Grassi, A., Flé, M., Bouchard,
 350 G., Plotnikov, I., Aunai, N., Dargent, J., Riconda, C., & Grech, M. (2018). Smilei :
 351 A collaborative, open-source, multi-purpose particle-in-cell code for plasma simulation.
 352 *Computer Physics Communications*, 222, 351–373. [https://doi.org/https://doi.org/10.](https://doi.org/https://doi.org/10.1016/j.cpc.2017.09.024)
 353 [1016/j.cpc.2017.09.024](https://doi.org/https://doi.org/10.1016/j.cpc.2017.09.024)
- 354 Duclous, R., Dubroca, B., Filbet, F., & Tikhonchuk, V. (2009). High order resolution of the
 355 maxwell-fokker-planck-landau model intended for ICF applications. *Journal of Computa-*
 356 *tional Physics*, 228(14), 5072–5100. [https://doi.org/https://doi.org/10.1016/j.jcp.2009.](https://doi.org/https://doi.org/10.1016/j.jcp.2009.04.005)
 357 [04.005](https://doi.org/https://doi.org/10.1016/j.jcp.2009.04.005)
- 358 Fried, B. D., & Conte, S. D. (1961). Elsevier.
- 359 Fromm, J. E. (1968). A method for reducing dispersion in convective difference schemes.
 360 *Journal of Computational Physics*, 3(2), 176–189. [https://doi.org/https://doi.org/10.](https://doi.org/https://doi.org/10.1016/0021-9991(68)90015-6)
 361 [1016/0021-9991\(68\)90015-6](https://doi.org/https://doi.org/10.1016/0021-9991(68)90015-6)
- 362 Godunov, S. K. (1959). Eine differenzenmethode für die näherungsberechnung unstetiger
 363 lösungen der hydrodynamischen gleichungen. *Mat. Sb., Nov. Ser.*, 47, 271–306.
- 364 Gould, R. W., O’Neil, T. M., & Malmberg, J. H. (1967). Plasma wave echo. *Phys. Rev.*
 365 *Lett.*, 19, 219–222. <https://doi.org/https://doi.org/10.1103/PhysRevLett.19.219>
- 366 Joglekar, A. S., & Levy, M. C. (2020). VlaPy: A python package for eulerian vlasov-poisson-
 367 fokker-planck simulations. *Journal of Open Source Software*, 5(53), 2182. [https://doi.](https://doi.org/https://doi.org/10.21105/joss.02182)
 368 [org/10.21105/joss.02182](https://doi.org/https://doi.org/10.21105/joss.02182)
- 369 Landau, L. D., & Lifshitz, E. M. (1981). *Physical kinetics* (Vol. 10). Pergamon Press.
- 370 Lax, P., & Wendroff, B. (1960). Systems of conservation laws. *Communications on Pure*
 371 *and Applied Mathematics*, 13(2), 217–237. [https://doi.org/https://doi.org/10.1002/cpa.](https://doi.org/https://doi.org/10.1002/cpa.3160130205)
 372 [3160130205](https://doi.org/https://doi.org/10.1002/cpa.3160130205)
- 373 Liu, X.-D., Osher, S., & Chan, T. (1994). Weighted essentially non-oscillatory schemes.
 374 *Journal of Computational Physics*, 115(1), 200–212. [https://doi.org/https://doi.org/10.](https://doi.org/https://doi.org/10.1006/jcph.1994.1187)
 375 [1006/jcph.1994.1187](https://doi.org/https://doi.org/10.1006/jcph.1994.1187)
- 376 Roe, P. L. (1986). Characteristic-based schemes for the euler equations. *Annual Review of*
 377 *Fluid Mechanics*, 18(1), 337–365. <https://doi.org/https://doi.org/10.1146/annurev.fl.18.010186.002005>
- 378 Sagdeev, R. Z., & Galeev, A. A. (1969). *Nonlinear Plasma Theory*. W. A. Benjamin, Inc.,
 379 New York.

- 380 Touati, M., Feugeas, J.-L., Nicolai, P., Santos, J. J., Gremillet, L., & Tikhonchuk, V. T.
381 (2014). A reduced model for relativistic electron beam transport in solids and dense
382 plasmas. *New Journal of Physics*, 16(7), 073014. [https://doi.org/10.1088/1367-2630/](https://doi.org/10.1088/1367-2630/16/7/073014)
383 [16/7/073014](https://doi.org/10.1088/1367-2630/16/7/073014)
- 384 Tzoufras, M., Bell, A. R., Norreys, P. A., & Tsung, F. S. (2011). A vlasov–fokker–planck code
385 for high energy density physics. *Journal of Computational Physics*, 230(17), 6475–6494.
386 [https://doi.org/https://doi.org/10.1016/j.jcp.2011.04.034](https://doi.org/10.1016/j.jcp.2011.04.034)
- 387 van Leer, B. (1979). Towards the ultimate conservative difference scheme. V. A second-
388 order sequel to godunov’s method. *Journal of Computational Physics*, 32(1), 101–136.
389 [https://doi.org/https://doi.org/10.1016/0021-9991\(79\)90145-1](https://doi.org/10.1016/0021-9991(79)90145-1)
- 390 Van Leer, B. (1977). Towards the ultimate conservative difference scheme III. Upstream-
391 centered finite-difference schemes for ideal compressible flow. *Journal of Computational*
392 *Physics*, 23(3), 263–275. [https://doi.org/https://doi.org/10.1016/0021-9991\(77\)](https://doi.org/10.1016/0021-9991(77)90094-8)
393 [90094-8](https://doi.org/10.1016/0021-9991(77)90094-8)
- 394 Yee, K. (1966). *IEEE Transactions on Antennas and Propagation*, 14(3), 302–307. [https://doi.org/https://doi.org/10.1109/TAP.1966.1138693](https://doi.org/10.1109/TAP.1966.1138693)
395 [/doi.org/10.1109/TAP.1966.1138693](https://doi.org/10.1109/TAP.1966.1138693)

DRAFT